J|A|C|S ARTICLES

Published on Web 07/20/2009

Modeling Metal Cation-Phosphate Interactions in Nucleic Acids: Activated Dissociation of Mg^+, Al^+, Cu^+, and Zn^+ Complexes of Triethyl Phosphate

Chunhai Ruan and M. T. Rodgers*

Department of Chemistry, Wayne State University, Detroit, Michigan 48202

Received November 26, 2008; E-mail: mrodgers@chem.wayne.edu

Abstract: Threshold collision-induced dissociation techniques are employed to determine the activation energies (AEs) and bond dissociation energies (BDEs) of metal cation-triethyl phosphate complexes, M^+(TEP), where $M^+ = Mg^+$, Al^+, Cu^+, and Zn^+. Activated dissociation resulting in loss of ethene, C_2H_4, corresponds to the primary and lowest energy pathway for all four systems examined. Sequential loss of additional C_2H_4 molecules and loss of the intact TEP ligand is also observed at elevated energies. Theoretical calculations at the B3LYP/6-31G* level of theory are used to determine the structures, vibrational frequencies, and rotational constants of neutral TEP and the M^+(TEP) complexes, transition states, intermediates, and products of the activated dissociation of these complexes. Theoretical AEs and BDEs are determined from single point energy calculations at the B3LYP/6-311+G(2d,2p) level using the B3LYP/6-31G* optimized geometries. The agreement between the calculated and measured AEs for elimination of C_2H_4 is excellent for all four systems. In contrast, less satisfactory agreement between theory and experiment is found for the M^+−TEP BDEs and may indicate limitations in the competitive model used to analyze these high energy dissociation pathways. The influence of the valence orbital occupation of the metal cation on the binding and activation propensities for elimination of ethene from TEP is examined. The binding of metal cations to TEP is compared to that of the nucleobases to assess the binding preferences of metal cations to nucleic acids.

Introduction

Nucleic acids are constructed from nucleobases (adenine, guanine, cytosine, thymine, and uracil) that are attached to a ribose (or deoxyribose)-phosphate backbone by an *N*-glycosidic linkage.[1] Thymine is found in DNA, while uracil is found in RNA. Nucleic acids play critical roles in the storage, transmission, and expression of genetic information. Metal cation binding to nucleic acids results in important interactions that influence the structure and mediate the functions of nucleic acids, for example, cross-linking, degradation, phosphodiester cleavage/strand scission, stabilization (destabilization), and mispairing.[2] Cis-platin ($Cl_2Pt(NH_3)_2$) and several other metal−ligand complexes have been shown to interact with nucleic acids and exhibit antitumor and antiviral activity.[3] All ribozymes require metal cations for stabilization of their structures and catalytic functions. Certain metal complexes can be used as probes for elucidating the structures and conformations along the DNA helix.[4] The biological importance of metal cation-nucleic acid interactions has aroused a great deal of interest in the study and characterization of these interactions in both model and real systems.[3]

Serving as link components in nucleic acids, phosphate esters connect thousands of base pairs to form large molecules that contain the genetic information. These phosphate groups are deprotonated such that nucleic acids are polyanions under physiological conditions. Positively charged metal cations bind to the phosphate groups and neutralize the negative charges on the nucleic acids. A specific range of counterion concentration is required to prevent the denaturization of nucleic acids.[5] Alkali and alkaline earth metal cation binding is mainly noncovalent, relatively weak, and occurs preferentially to the phosphate backbone of nucleic acids.[6−8] In contrast, transition metal cation binding is generally stronger and more complicated than alkali and alkaline earth metal cation binding due to the involvement of the valence d orbital electrons in the binding and may induce profound effects on the structure and function of nucleic acids. Transition metal cations are capable of binding to multiple parts of a nucleic acid, including the phosphate groups and nucleobases via the heteroatoms and aromatic rings. In aqueous solution, the preference for phosphate over base association was found to decrease in the order: $Mg^{2+} > Co^{2+} > Ni^{2+} > Mn^{2+} > Zn^{2+} > Cd^{2+} > Cu^{2+}$.[9] This trend in the relative binding affinities is consistent with the hardest metal ions exhibiting the greatest preference for binding to the phosphate backbone. In the solution phase, the binding of metal cations to the phosphate groups of calf thymus DNA was studied using electrophoresis. The binding

(1) Bertini, I.; Gray, H. B.; Lippard, S. J.; Valentine, J. S. *Bioinorganic Chemistry*; University Science Books: Mill Valley, CA, 1994; p 455.
(2) Eichhorn, G. L.; Butzow, J. J. *Proc. Int. Symp. Biomol. Struct. Interactions, Suppl. J. Biosci.* **1985**, *8*, 527.
(3) Spiro, T. G. *Nucleic Acid-Metal Ion Interactions*; Wiley: New York, 1980; Vol. 1.
(4) Barton, J. K. *Science* **1986**, *233*, 727.
(5) Schildkraut, C.; Lifson, S. *Biopolymers* **1965**, *3*, 195.
(6) Eichhorn, G. L. *Adv. Inorg. Biochem.* **1981**, *3*, 1.
(7) Martin, R. B. *Acc. Chem. Res.* **1985**, *18*, 32.
(8) Sigel, H. *Chem. Soc. Rev.* **1993**, *22*, 255.
(9) Eichhorn, G. L.; Shin, Y. A. *J. Am. Chem. Soc.* **1968**, *90*, 7323.

10.1021/ja8092357 CCC: $40.75

affinities of these metal cations were found to follow the order $Mn^{2+} > Mg^{2+} > Ca^{2+}$ and $Li^+ > Na^+ > K^+$.[10]

There has been a great deal of interest in the characterization of metal cation−phosphate interactions in nucleic acids. Metal cation binding to the phosphate group may not only stabilize the phosphate backbone of nucleic acids, but may also aid in catalyzing the cleavage of the phosphate ester linkages by stabilizing intermediates during the catalysis. The binding of metal cations to the phosphate backbone has been shown to lead to selective cleavage of the 3′-phosphodiester linkage in some cases[11−14] via a mechanism analogous to 1,2-elimination reactions commonly observed in the pyrolysis of esters.[15] Sargeson et al. studied metal cation promoted phosphate ester hydrolysis and found that the rate of hydrolysis is modulated by the size of the metal cation and the ease of formation of a four-membered chelate ring.[16] Bruice found a pentacoordinate intermediate in the catalysis of alkyl phosphate diesters.[17] Metal cation−phosphate interactions also play a role in protein−nucleic acid recognition mechanisms.[18−20] Sigler and co-workers found that Ca^{2+} may bridge carboxylate and phosphate groups and hypothesized that these interactions may be involved in the recognition of the Trp repressor and operator.[19]

Metal cation binding significantly influences the physical properties, conformations, and functionality of nucleic acids. The phosphate groups and nucleobases are the major metal binding sites of nucleic acids. Cerda and Wesdemiotis determined alkali metal cation ($M^+ = Li^+$, Na^+, and K^+) binding affinities of the nucleobases (guanine (G), cytosine (C), adenine (A), thymine (T), and uracil (U)) using the kinetic method.[21] The interaction of alkali metal cations ($M^+ = Li^+$, Na^+, and K^+) with U, T, and A was also studied by threshold collision-induced dissociation (TCID) techniques in our group.[22] Yang et al. determined the bond energy of Mg^+ to U and T using photodissociation methods.[23] Hobza et al. studied the interaction of G and A with various mono- and divalent metal cations (Li^+, Na^+, K^+, Rb^+, Cs^+, Cu^+, Ag^+, Au^+, Mg^{2+}, Ca^{2+}, Sr^{2+}, Ba^{2+}, Zn^{2+}, Cd^{2+}, Hg^{2+}) using ab initio calculations.[24] In our previous studies, the influence of the d orbital occupation on metal cation binding to A was studied using TCID techniques and electronic structure theory.[25] Grand et al. determined the Cu^+ affinity of the DNA and RNA nucleobases using density functional theory calculations.[26] Detailed knowledge regarding the metal cation binding modes of phosphate esters and the nucleobases (G, C, A, T, and U) and their propensities to activated the phosphate ester would greatly improve the understanding on how metal cations interact with nucleic acid structures and influence their structure, stability, and reactivity. Coupling of studies of metal cation binding to the nucleobases and model phosphate esters should allow prediction of the most favorable metal cation binding sites to nucleic acids, and determine the influence of metal cations on the reactivity and dissociation mechanisms of metal cation-nucleic acid complexes.

In previous studies in our laboratory,[27,28] trimethyl phosphate (TMP) and triethyl phosphate (TEP) were used as simple models for the phosphate backbone of nucleic acids and their alkali metal cation binding affinities were determined. No activated dissociation was observed in the collision-induced dissociation (CID) of these alkali metal cation-phosphate ester complexes. In the present study, this work is expanded to include Mg^+, Al^+, Cu^+ and Zn^+ binding to TEP. By studying the interactions between metal cations and phosphate esters, we seek to determine absolute metal cation binding affinities of these phosphate esters and determine how metal cation binding influences the structure and propensity for activation of the phosphate ester bonds. The kinetic energy dependences of the CID of four M^+(TEP) complexes, where $M^+ = Mg^+$, Al^+, Cu^+, and Zn^+, with Xe are examined using a guided ion beam tandem mass spectrometer. The cross sections for the CID processes observed for each complex are analyzed using methods previously developed.[29] The trends in the M^+−TEP bond dissociation energies (BDEs) and activation energies (AEs) for elimination of ethene, C_2H_4, from these M^+(TEP) complexes are elucidated. The influence of the valence orbital occupation of the metal cation on the binding and its propensity to activate the phosphate ester linkages is examined.

Experimental Section

General Procedures. Cross sections for CID of four M^+(TEP) complexes, where $M^+ = Mg^+$, Al^+, Cu^+, and Zn^+, are measured using a guided ion beam tandem mass spectrometer that has been described in detail previously.[30] Metal cations are generated in a continuous dc discharge by argon ion sputtering of a cathode made of the metal of interest. Typical operating conditions of the discharge are 1.3−2.7 kV and 13−27 mA for cation production in a flow of roughly 10% argon in helium. The complexes are generated in a flow tube ion source by condensation of the metal cation and neutral TEP molecule. These complexes are collisionally stabilized and thermalized by in excess of 10^5 collisions with the He and Ar bath gases such that the internal energies of the ions emanating from the source region are believed to be well described by a Maxwell−Boltzmann distribution at room temperature. The ions are effusively sampled from the source, focused, accelerated, and focused into a magnetic sector momentum analyzer for mass analysis. Mass-selected ions are decelerated to a desired kinetic energy and focused into an octopole ion beam guide. The octopole passes through a static gas cell containing Xe at low pressure (0.05−0.20 mTorr) to ensure that multiple ion-neutral collisions are improbable. The octopole ion guide acts as an efficient trap for ions in the radial direction. Therefore, loss of scattered reactant and product ions in the octopole region is almost entirely eliminated.[31−33] Xe is used here, and in general for all of our CID

(10) Ross, P. D.; Scruggs, R. L. *Biopolymers* **1964**, *2*, 79.
(11) Phillips, D. R.; McCloskey, J. A. *Int. J. Mass Spectrom. Ion Proc.* **1993**, *128*, 61.
(12) Rodgers, M. T.; Campbell, S.; Marzluff, E. M.; Beauchamp, J. L. *Int. J. Mass Spectrom. Ion Proc.* **1995**, *148*, 1.
(13) Rodgers, M. T.; Campbell, S.; Beauchamp, J. L. *Int. J. Mass Spectrom. Ion Proc.* **1997**, *161*, 193.
(14) Linscheid, M.; Burlingame, A. L. *Org. Mass Spectrom.* **1983**, *18*, 245.
(15) Ratchford, W. P. *Organic Syntheses, Coll.* **1955**, *3*, 30. Ratchford, W. P. *Organic Syntheses, Coll.* **1949**, *29*, 2.
(16) Hendry, P.; Sargeson, A. M. *J. Am. Chem. Soc.* **1989**, *111*, 2521.
(17) Dempcy, R. O.; Bruice, T. C. *J. Am. Chem. Soc.* **1994**, *116*, 4511.
(18) Matthews, B. W. *Nature* **1988**, *335*, 294.
(19) Otwinowski, Z.; Schevitz, R. W.; Zhang, R.-G.; Lawson, C. L.; Joachimiak, A.; Marmorstein, R. Q.; Luisi, B. F.; Sigler, P. B. *Nature* **1988**, *335*, 321.
(20) Anderson, J. E.; Ptashne, M.; Harrison, S. C. *Nature* **1987**, *326*, 846.
(21) Cerda, B. A.; Wesdemiotis, C. *J. Am. Chem. Soc.* **1996**, *118*, 11884.
(22) Rodgers, M. T.; Armentrout, P. B. *J. Am. Chem. Soc.* **2000**, *122*, 8548.
(23) Liu, H.; Sun, J.-L.; Hu, Y.; Han, K.-L.; Yang, S. *Chem. Phys. Lett.* **2004**, *389*, 342.
(24) Burda, J. V.; Sponer, J.; Hobza, P. *J. Phys. Chem.* **1996**, *100*, 7250.
(25) Rodgers, M. T.; Armentrout, P. B. *J. Am. Chem. Soc.* **2002**, *124*, 2678.
(26) Russo, N.; Toscano, M.; Grand, A. *J. Mass Spectrom.* **2003**, *38*, 265.
(27) Ruan, C.; Huang, H.; Rodgers, M. T. *J. Am. Soc. Mass Spectrom.* **2008**, *19*, 305.
(28) Ruan, C.; Huang, H.; Rodgers, M. T. *J. Phys. Chem. A* **2007**, *111*, 13521.
(29) Rodgers, M. T.; Ervin, K. M.; Armentrout, P. B. *J. Chem. Phys.* **1997**, *106*, 4499.
(30) Rodgers, M. T. *J. Phys. Chem. A* **2001**, *105*, 2374.
(31) Teloy, E.; Gerlich, D. *Chem. Phys.* **1974**, *4*, 417.

measurements, because it is heavy and polarizable and therefore leads to more efficient kinetic to internal energy transfer in the CID process.[34−36] Products and unreacted beam ions drift to the end of the octopole, where they are focused into a quadrupole mass filter for mass analysis, and subsequently detected with a secondary electron scintillation detector and standard pulse counting techniques.

Ion intensities are converted to absolute cross sections using a Beers' law analysis as described previously.[37] Absolute uncertainties in cross section magnitudes are estimated to be ±20%, which are largely the result of errors in the pressure measurement and the length of the interaction region. Relative uncertainties are approximately ±5%.

Ion kinetic energies in the laboratory frame, E_{lab}, are converted to energies in the center of mass frame, E_{CM}, using the formula $E_{CM} = E_{lab}m/(m + M)$, where M and m are the masses of the ionic and neutral reactants, respectively. All energies reported below are in the center-of-mass frame unless otherwise noted. The absolute zero and distribution of the ion kinetic energies are determined using the octopole ion guide as a retarding potential analyzer as previously described.[37] The distribution of ion kinetic energies is nearly Gaussian with a fwhm between 0.2 and 0.4 eV (lab) for these experiments. The uncertainty in the absolute energy scale is ±0.05 eV (lab).

Pressure-dependent studies of all CID cross sections examined here were performed because multiple collisions can influence the shape of CID cross sections and the threshold regions are most sensitive to these effects. Data free from pressure effects are obtained by extrapolating to zero pressure of the neutral reactant, Xe, as described previously.[38] Thus, cross sections subjected to thermochemical analysis are the result of single bimolecular encounters.

Quantum Chemical Calculations. To obtain model structures, vibrational frequencies, and energetics for neutral TEP, the M^+(TEP) complexes, transition states (TSs), intermediates, and products of the activated dissociation of the M^+(TEP) complexes, simulated annealing and quantum chemical calculations were performed using HyperChem[39] and Gaussian 03,[40] respectively. Initially, 100 cycles of simulated annealing were performed using HyperChem to find reasonable candidates for the ground state structure of TEP and each M^+(TEP) complex. Geometry optimizations and frequency analyses were then performed using Gaussian 03 at the B3LYP/6-31G* level for all plausible low-energy structures of neutral TEP and the M^+(TEP) complexes. For all of the complexes studied here, the spin state was assumed to be the same as the spin state of the ground state of the bare metal cation (i.e., Mg^+ doublet, Al^+ singlet, Cu^+ singlet, and Zn^+ doublet). The calculated vibrational frequencies were scaled by a factor of 0.9804 and are listed in Table 1S of the Supporting Information. Table 2S (Supporting Information) lists the rotational constants for the ground state conformations. Single point energy calculations at the B3LYP/6-311+G(2d,2p) level of theory were performed using Gaussian 03 and the B3LYP/6-31G* optimized geometries. To obtain accurate energetics, zero point energy (ZPE) corrections were included in the calculation of the theoretical AEs and BDEs. Basis set superposition error (BSSE) corrections in the full counterpoise approximation were also included in the calculated BDEs.[41,42]

Two pathways for activated dissociation leading to elimination of ethene from the M^+(TEP) complexes were found. Dissociation via a 6-membered ring transition state (TS_{6M}) or a 4-membered ring transition state (TS_{4M}) were carefully mapped from the reactant M^+(TEP) complexes to the dissociation products, M^+(DEP) and C_2H_4 (where DEP is diethyl phosphate) at the B3LYP/6-311+G(2d,2p)//B3LYP/6-31G* level of theory.

The polarizability of the ligand is one of the key factors that influence the strength of metal cation-ligand binding. A theoretical calculation of the polarizability of TEP based on a dipole electric field was carried out at the PBE0/6-311+G(2d,2p) level of theory and used in the thermochemical analysis of the experimental data. This level of theory was chosen because it has been shown to provide polarizabilities that are in better agreement with experimental values than polarizabilities computed using the B3LYP functional employed here for the structures and energetics of these systems.[43]

Thermochemical Analysis. The threshold regions of the CID cross sections for activated dissociation resulting in elimination of C_2H_4 and simple CID leading to loss of the intact TEP ligand are modeled using eq 1,

$$\sigma(E) = \sigma_0 \sum_i g_i(E + E_i - E_0)^n/E \quad (1)$$

where σ_0 is an energy independent scaling factor, E is the relative translational energy of the reactants, E_0 is the threshold for reaction of the ground electronic and ro-vibrational state, and n is an adjustable parameter that describes the efficiency of kinetic to internal energy transfer.[44] The summation is over the ro-vibrational states of the reactant ions, i, where E_i is the excitation energy of each ro-vibrational state and g_i is the population of those states ($\Sigma g_i = 1$).

For all four M^+(TEP) systems, the onsets for activated dissociation leading to the sequential elimination of one, two, and three ethene molecules occur at lower energies than simple CID to produce the bare metal cation. To extract accurate threshold values and examine the effects of competition on the measured CID cross sections, a statistical model based on eq 1 for simultaneous analyses of the activated dissociation and simple CID cross sections, eq 2, is used in the thermochemical analysis of all systems.[45] The results of these competitive analyses are compared with that for individual modeling of the activated dissociation and simple CID pathways.

$$\sigma_j(E) = \frac{n\sigma_{0,j}}{E} \sum_i g_i \int_0^{E+E_i-E_0} \frac{k_j(E^*)}{k_{tot}(E^*)} \times [1 - e^{-k_{tot}(E^*)\tau}](\Delta E)^{n-1} d(\Delta E) \quad (2)$$

The indices j refer to a particular product channel and $k_{tot} = \Sigma k_j$, where all rate constants are calculated using Rice-Ramsperger-Kassel-Marcus (RRKM) theory. The ratio of dissociation rates k_j/k_{tot} introduces the coupling between product channels j. The scaling factors $\sigma_{0,j}$ are ideally the same for all product channels, while individual scaling is needed to accurately reproduce the cross section magnitudes in some cases. E^* is the internal energy of the energized molecule after collision, $E^* = E + E_i - \Delta E$, where E and E_i are defined in eq 1 and ΔE is the energy that remains in translation after collision between the M^+(TEP) complex and Xe.

(32) Gerlich, D. Diplomarbeit, University of Freiburg, Federal Republic of Germany, 1971.
(33) Gerlich, D. In *State-Selected and State-to-State Ion−Molecule Reaction Dynamics, Part I, Experiment*; Ng, C.-Y., Baer, M., Eds.;Advances in Chemical Physics Series; Wiley: New York, 1992; Vol. 82, p 1.
(34) Dalleska, N. F.; Honma, K.; Armentrout, P. B. *J. Am. Chem. Soc.* **1993**, *115*, 12125.
(35) Aristov, N.; Armentrout, P. B. *J. Phys. Chem.* **1986**, *90*, 5135.
(36) Hales, D. A.; Armentrout, P. B. *J. Cluster Sci.* **1990**, *1*, 127.
(37) Ervin, K. M.; Armentrout, P. B. *J. Chem. Phys.* **1985**, *83*, 166.
(38) Dalleska, N. F.; Honma, K.; Sunderlin, L. S.; Armentrout, P. B. *J. Am. Chem. Soc.* **1994**, *116*, 3519.
(39) *HyperChem Computational Chemistry Software Package*, Version 5.0; Hypercube Inc: Gainsville, FL, 1997.
(40) Frisch, M. J.; et al. *Gaussian 03*, Revision C.01; Gaussian, Inc.: Wallingford, CT, 2004. See Supporting Information for full reference.
(41) Boys, S. F.; Bernardi, R. *Mol. Phys.* **1979**, *19*, 553.
(42) van Duijneveldt, F. B.; van Duijneveldt-van de Rijdt, J. G. C. M.; van Lenthe, J. H. *Chem. Rev.* **1994**, *94*, 1873.
(43) Smith, S. M.; Markevitch, A. N.; Romanov, D. A.; Li, X.; Levis, R. J.; Schlegel, H. B. *J. Phys. Chem. A* **2004**, *108*, 11063.
(44) Muntean, F.; Armentrout, P. B. *J. Chem. Phys.* **2001**, *115*, 1213.
(45) Rodgers, M. T.; Armentrout, P. B. *J. Chem. Phys.* **1998**, *109*, 1787.

The Beyer−Swinehart algorithm is used to evaluate the density of ro-vibrational states,[46−48] and the relative populations, g_i, are calculated for a Maxwell−Boltzmann distribution at 298 K, the internal temperature of the reactants. The average internal energies at 298 K of neutral TEP and the M^+(TEP) complexes are also given in Table 1S (Supporting Information). We have estimated the sensitivity of our analyses to the deviations from the true frequencies by scaling the vibrational frequencies (prescaled by 0.9804) by ± 10%. The corresponding change in the average vibrational energy is taken to be an estimate of one standard deviation of the uncertainty in the vibrational energy (Table 1S, Supporting Information) and is included in the uncertainties listed with the threshold values.

We also consider the possibility that the collisionally activated M^+(TEP) complexes do not dissociate on the time scale of the experiment ($\sim 10^{-4}$ s) by including statistical theories for unimolecular dissociation, specifically RRKM theory, into eqs 1 and 2 as described in detail elsewhere.[29,49] The ro-vibrational frequencies appropriate for the energized molecules and the TSs leading to dissociation are given in Tables 1S and 2S (Supporting Information). For the simple CID processes, we assume that the TSs are loose and product-like because the interaction between the metal cation and the TEP ligand is largely electrostatic. The TS vibrations used are the frequencies corresponding to the molecular product, TEP. The transitional frequencies, those that become rotations of the completely dissociated products, are treated as rotors corresponding to a phase space limit (PSL) as described in detail elsewhere.[29] For the activated dissociation processes, two tight TSs are found, TS_{6M} and TS_{4M}. The TS_{6M} pathway is found to provide a lower-energy pathway for elimination of ethene from the M^+(TEP) complexes for all metal cations except Al^+, where calculations suggest that the TS_{4M} pathway is favored. The molecular parameters of both the TS_{6M} and TS_{4M} structures are used in the data analysis for the four M^+(TEP) systems to accurately establish which TS best reproduces the data and provides the lowest energy pathway to the products.

The models represented by eqs 1 and 2 are expected to be appropriate for translationally driven reactions[50] and have been shown to reproduce CID cross sections well. The models of eqs 1 and 2 are convoluted with the kinetic energy distributions of the M^+(TEP) complex and Xe, and a nonlinear least-squares analysis of the data is performed to give optimized values for the parameters σ_0, E_0, and n. The errors in the measured thresholds are estimated from the range of values determined for the zero-pressure-extrapolated data sets, variations associated with uncertainties in the vibrational frequencies (±10% scaling as described above), and the error in the absolute energy scale, ±0.05 eV (lab). For analyses that include the RRKM lifetime analysis, the uncertainties in the E_0(PSL) and $E_0(TS_{6M})$ values also include the effects of increasing and decreasing the time assumed available for dissociation ($\sim 10^{-4}$ s) by a factor of 2.

Equations 1 and 2 explicitly include the internal energy of the ion, E_i. All energy available is treated statistically because the ro-vibrational energy of the reactant complex is redistributed throughout the M^+(TEP) complex upon impact with Xe. Because the simple CID processes examined here correspond to noncovalent bond cleavage reactions, the E_0(PSL) values determined by analysis with eqs 1 and 2 can be equated to 0 K BDEs.[51,52] For the activated dissociation pathways, the $E_0(TS_{6M})$ values determined by analysis with eqs 1 and 2 correspond to 0 K AEs for elimination of C_2H_4.

(46) Beyer, T. S.; Swinehart, D. F. *Commun. ACM* **1973**, *16*, 379.
(47) Stein, S. E.; Rabinovitch, B. S. *J. Chem. Phys.* **1973**, *58*, 2438.
(48) Stein, S. E.; Rabinovitch, B. S. *Chem. Phys. Lett.* **1977**, *49*, 183.
(49) Khan, F. A.; Clemmer, D. E.; Schultz, R. H.; Armentrout, P. B. *J. Phys. Chem.* **1993**, *97*, 7978.
(50) Chesnavich, W. J.; Bowers, M. T. *J. Phys. Chem.* **1979**, *83*, 900.
(51) See, for example, Figure 1 in Dalleska, N. F.; Honma, K.; Armentrout, P. B. *J. Am. Chem. Soc.* **1993**, *115*, 12125.
(52) Armentrout, P. B.; Simons, J. *J. Am. Chem. Soc.* **1992**, *114*, 8627.

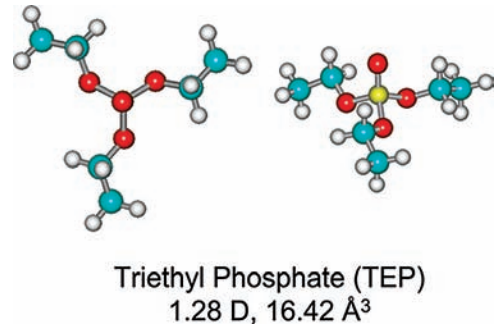

Figure 1. B3LYP/6-31G* optimized structure of triethyl phosphate (TEP). Two views of this structure are shown. The B3LYP/6-311+G(2d,2p) dipole moment and PBE0/6-311+G(2d,2p) isotropic molecular polarizability calculated here are also shown.

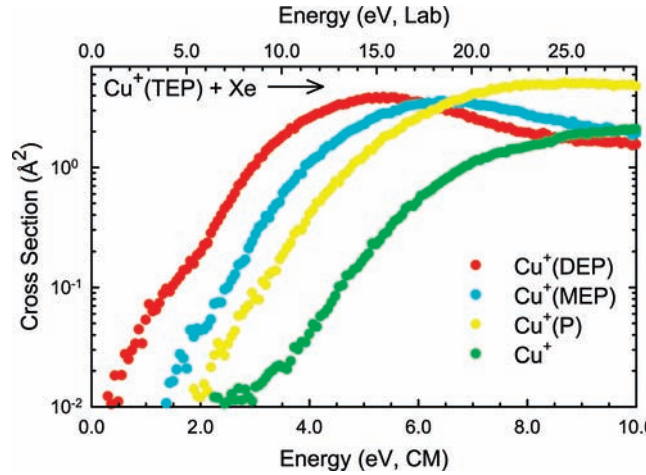

Figure 2. Cross section for collision-induced dissociation of Cu^+(TEP) with Xe as a function of collision energy in the center-of-mass frame (lower *x*-axis) and laboratory frame (upper *x*-axis). Data are shown for a Xe pressure of 0.2 mTorr.

Results

Cross Sections for Collision-Induced Dissociation. Experimental cross sections were obtained for the interaction of Xe with four M^+(TEP) complexes, where $M^+ = Mg^+$, Al^+, Cu^+, and Zn^+. Figure 2 shows representative data for the Cu^+(TEP) complex. The other M^+(TEP) complexes exhibit similar behavior and are shown in Figure 1S of the Supporting Information. Activated dissociation resulting in elimination of ethene, C_2H_4, corresponds to the primary and lowest energy CID pathway for all four systems, reaction 3,

$$M^+(TEP) + Xe \rightarrow M^+(DEP) + C_2H_4 + Xe \qquad (3)$$

where M^+(DEP) is the metal cation-diethyl phosphate complex. Sequential loss of one and two additional C_2H_4 molecules is also observed at elevated energies, reactions 4−5,

$$M^+(TEP) + Xe \rightarrow M^+(MEP) + 2\,C_2H_4 + Xe \qquad (4)$$

$$M^+(TEP) + Xe \rightarrow M^+(P) + 3\,C_2H_4 + Xe \qquad (5)$$

where M^+(MEP) and M^+(P) are the metal cation-monoethyl phosphate and metal cation-phosphoric acid complexes, respectively. Simple CID resulting in loss of the intact TEP ligand is also observed at elevated energies for all four M^+(TEP) complexes, reaction 6.

$$M^+(TEP) + Xe \rightarrow M^+ + TEP + Xe \quad (6)$$

Two additional dissociation pathways are observed at elevated energies in the CID of the Zn^+(TEP) complex. The ethyl cation, $C_2H_5^+$, begins to appear at an apparent threshold near 5 eV as the Zn^+(DEP) product cross section begins to decline, suggesting that this dissociation pathway, reaction 7, competes with reaction 3.

$$Zn^+(TEP) + Xe \rightarrow Zn(DEP\text{-}H) + C_2H_5^+ + Xe \quad (7)$$

Loss of CH_3CO from the Zn^+(MEP) product, reaction 8, is also observed as a minor high energy sequential dissociation pathway.

$$Zn^+(MEP) \rightarrow Zn^+(H_3PO_3) + CH_3CHO \quad (8)$$

Theoretical Results. Theoretical structures for the ground states, transition states, intermediates, and products of the activated dissociation of the M^+(TEP) complexes were calculated as described above. The Cartesian coordinates of the geometry-optimized structures for all species are given in Table 3S (Supporting Information) for the activated dissociation via the 6-membered ring transition state, while the structures associated with the activated dissociation via the 4-membered ring transition state are given in Table 4S (Supporting Information). Tables 5S−7S (Supporting Information) provide key geometrical parameters of the optimized geometries for TEP, the M^+(TEP) complexes, and the TS_{6M} and TS_{4M} transition states for activated dissociation. In our previous work,[28] the ground state structure of neutral TEP was found to be a completely staggered structure to minimize repulsion between the three ethyl groups, as shown in Figure 1. The ground state and low-energy conformations for Cu^+(TEP) are shown in Figure 3, while the analogous structures for the other M^+(TEP) complexes are shown in the Supporting Information as Figure 2S.

M^+(TEP) Complexes. Multiple stable low-energy conformers were found for the M^+(TEP) complexes. For all four M^+(TEP) complexes, the ground-state structures involve bidentate binding of the metal cation to the oxo and one of the alkoxy oxygen atoms forming a 4-membered chelate ring, similar to that found for the alkali metal cation M^+(TEP) and M^+(TMP) complexes (Figures 3 and 2S, Supporting Information).[27,28] The ethyl group of the bound alkoxy group is oriented away from the oxo oxygen to allow the alkoxy oxygen lone pairs to interact with the metal cation and thereby provide additional stabilization to the complex, while the other two ethyl groups remain staggered to minimize repulsion with each other. Rotation of the bound alkoxy group of the ground state conformer away from the metal cation results in a configuration in which the metal cation only interacts with the oxo oxygen atom (Figure 3). Similar conformations are found for the other M^+(TEP) systems (Figure 2S, Supporting Information). The monodentate conformations are found to be 8.4, 5.3, 9.0, and 12.7 kJ/mol less stable than the ground state conformer for the Mg^+(TEP), Al^+(TEP), Cu^+(TEP), and Zn^+(TEP) complexes, respectively. In neutral TEP, the analogous rotation of one ethyl group results in a 5 kJ/mol increase in energy (destabilization).[28] This indicates that interaction with the second oxygen atom enhances the binding by ∼5% for all four M^+(TEP) systems.

The ground state structures computed for all four M^+(TEP) complexes are similar (Figures 3 and 2S, Supporting Information). The metal cation-oxo oxygen (M^+−O3) bond lengths vary between 1.763 and 1.925 Å and are significantly shorter than the metal cation-alkoxy oxygen (M^+−O4) bond lengths, which vary between 3.069 and 3.854 Å, respectively. The calculated M^+−TEP BDEs vary between 260.5 and 272.5 kJ/mol for these complexes. Upon binding to TEP, the P═O3 and C−O bonds are lengthened, while the P−O4, P−O5, and P−O6 bonds contract. The C−C and C−H bonds are essentially unaffected by metal cation binding for these complexes and are 1.512 and 1.094 Å, respectively. The metal cation is shifted away from the plane determined by the O3═P−O4 atoms, such that the ∠M^+O3PO4 dihedral angle varies from −19.7 to −41.9° across these complexes.

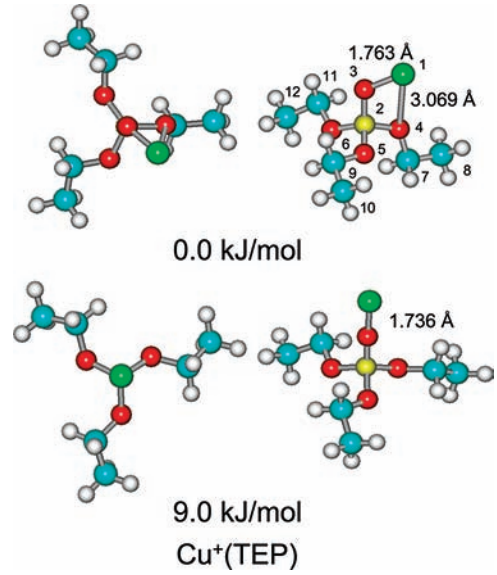

Figure 3. B3LYP/6-31G* optimized structures and B3LYP/6-311+G(2d,2p) relative stabilities of stable low-energy conformers of the Cu^+(TEP) complex. Two views of each structure are shown.

Table 1. B3LYP/6-311+G(2d,2p) Relative Stabilities (in kJ/mol) of Ground State M^+(TEP) Complexes, Transition States, Intermediates, and Products Involved in the Activated Dissociation of M^+(TEP) to Eliminate Ethene via 6-Membered and 4-Membered Ring TSs[a]

	relative energy (kJ/mol)			
species	Mg^+	Al^+	Cu^+	Zn^+
M^+ + TEP	264.5	267.4	276.1	272.0
M^+(TEP)	0.0	0.0	0.0	0.0
TS_{6M}	158.6	179.3	161.8	164.2
TS_{4M}	177.2	163.0	180.8	178.4
M^+(DEP)*·C_2H_4	97.7	131.2	122.5	106.7
M^+(DEP)* + C_2H_4	130.0	164.2	154.2	139.3
M^+(DEP)·C_2H_4	36.4	32.5	31.5	35.9
M^+(DEP) + C_2H_4	55.1	58.5	53.1	56.4

[a] B3LYP/6-31G* optimized geometries, including ZPE corrections with frequencies scaled by 0.9804.

Activated Dissociation of the M^+(TEP) Complexes. As discussed above, activated dissociation pathways are observed for all four M^+(TEP) complexes. To allow appropriate thermochemical analysis of the primary activated dissociation pathway, i.e., loss of C_2H_4 from the M^+(TEP) complexes, reactions 3, potential energy landscapes for the unimolecular dissociation of the M^+(TEP) complexes are mapped out. Results for all four M^+(TEP) complexes are summarized in Table 1. In particular, the relative energies of the reactant M^+(TEP) complexes and the rate-limiting TSs are determined as theoretical estimates for the AEs. Two pathways for elimination of C_2H_4

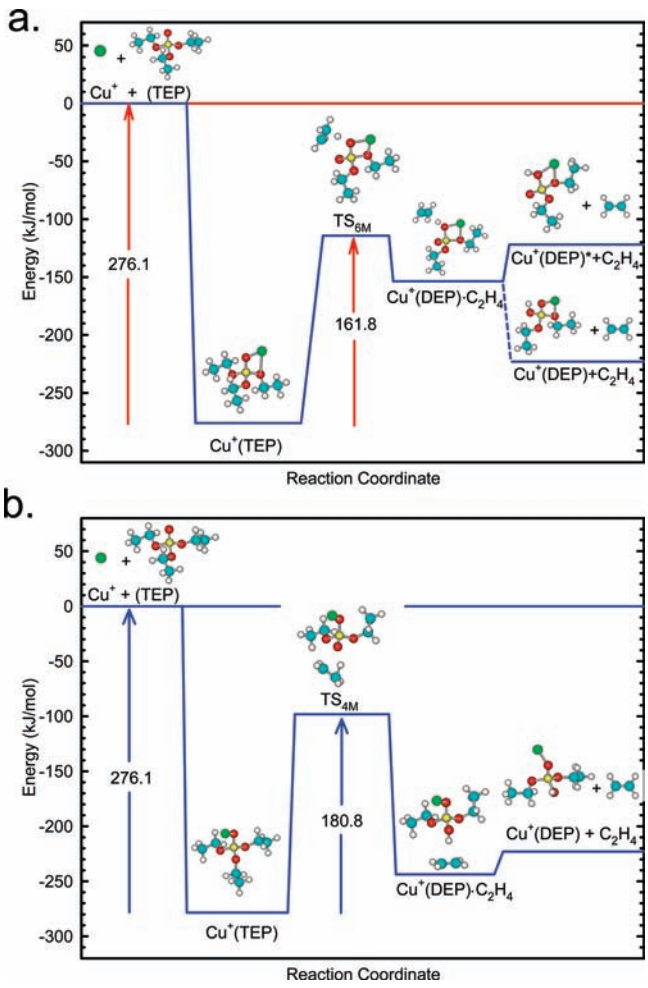

Figure 4. Potential energy landscape at 0 K for elimination of C_2H_4 from Cu^+(TEP) via a 6-membered ring transition state, TS_{6M} (a) and a 4-membered ring transition state, TS_{4M} (b). Energies are relative to the reactant Cu^+(TEP) complex and taken from theoretical calculations at the B3LYP/6-311+G(2d,2p) level of theory using the B3LYP/6-31G* optimized geometries including ZPE corrections.

from M^+(TEP) are found. The first pathway occurs via formation of a 6-membered ring TS, TS_{6M}, while the second pathway involves formation of a 4-membered ring TS, TS_{4M}. The potential energy landscapes for the TS_{6M} and TS_{4M} pathways of Cu^+(TEP) are shown in Figure 4. The potential energy landscapes for the analogous TS_{6M} and TS_{4M} pathways of the Mg^+(TEP), Al^+(TEP), and Zn^+(TEP) complexes are shown in Figure 3S of the Supporting Information. Geometrical parameters of the TS_{6M} and TS_{4M} transition state structures are summarized in Tables 6S and 7S (Supporting Information), respectively. Based on the calculated energetics, the TS_{6M} pathway is the lowest energy activated dissociation pathway for the Mg^+(TEP), Cu^+(TEP), and Zn^+(TEP) complexes, while the TS_{4M} pathway is the lowest energy pathway for Al^+(TEP).

In TS_{6M}, the metal cation interacts with the oxo and one of the alkoxy oxygen atoms in a bidentate fashion forming a 4-membered chelate ring similar to that of the reactant M^+(TEP) complex (Figures 4 and 3S, Supporting Information). One of the ethyl groups that are not involved in the binding of the metal cation is oriented upward forming a 6-membered ring with the oxo oxygen (O3═P−O6−C11−C12−H). This TS relaxes to an ion-neutral complex, M^+(DEP)*·C_2H_4, where M^+(DEP)* is an excited conformation of M^+(DEP), which dissociates to the corresponding products via a loose TS. TS_{6M} is the rate-limiting TS for this dissociation pathway. The Cartesian coordinates of the reactant complexes, TSs, intermediates, and products of the TS_{6M} pathway are summarized in Table 3S (Supporting Information).

Compared to the corresponding ground state structures, the M^+−O3 bond lengths of TS_{6M} slightly lengthen, while the M^+−O4 bond lengths shorten significantly. The M^+−O3 and M^+−O4 bond lengths are found to vary from 1.903 to 2.055 Å and 2.001 to 2.411 Å, respectively. The P−O3 and P−O4 bonds of TS_{6M} are slightly lengthened and vary from 1.591 to 1.621 Å and 1.625 to 1.656 Å, respectively. The P−O6 bond lengths shorten indicating the conversion from a P−O to P═O bond and vary from 1.485 to 1.490 Å. Similarly the C11−C12 bond lengths shorten indicating the conversion from a C−C to C═C bond and vary between 1.376 to 1.384 Å. The C11−O6 bond is significantly lengthened as this bond is cleaved in the products and varies from 2.491 to 2.582 Å. The C12−H bond is also lengthened and varies from 1.291 to 1.325 Å as this bond is also cleaved in the products. The O3−H bond lengths decrease indicating the formation of a new bond, but are still much longer than a typical O−H bond, and vary from 1.375 to 1.404 Å. The ∠M^+O3PO4 dihedral angle also decreases and varies from −5.8 to −14.3°.

In TS_{4M}, the metal cation again binds to TEP in a bidentate fashion forming a 4-membered chelate ring similar to that of the reactant M^+(TEP) complex and TS_{6M} (Figures 4 and 3S, Supporting Information). The ethyl group of the bound alkoxy oxygen atom is oriented away from the oxo oxygen and forms a 4-membered ring with the alkoxy oxygen (O4−C7−C8−H). This TS relaxes to an ion-neutral complex, M^+(DEP)·C_2H_4 that dissociates to the corresponding products via a loose TS with no barrier in excess of the endothermicity of dissociation. TS_{4M} is the rate-limiting TS for this pathway. The Cartesian coordinates of the reactant complexes, TSs, intermediates, and products of the TS_{4M} pathway are summarized in Tables 3S and 4S (Supporting Information).

Compared to the corresponding ground state structures, the M^+−O3 and M^+−O4 bond lengths of TS_{4M} are slightly shortened. The M^+−O3 and M^+−O4 bond lengths vary from 1.755 to 1.978 Å and 2.216 to 4.076 Å, respectively. The P═O3 bond lengths slightly lengthen upon metal cation binding and vary from 1.537 to 1.567 Å. The P−O4 and C7−C8 bond lengths contract slightly, the latter indicating the conversion from a C−C to a C═C bond, and vary from 1.516 to 1.563 Å and 1.391 to 1.392 Å, respectively. The C8−H and C7−O4 bond lengths lengthen markedly, as these bonds are cleaved in the products, and vary from 1.207 to 1.214 Å and 2.416 to 2.495 Å, respectively. The O4−H bond lengths decrease indicating the formation of a new bond, but are still much longer than a typical O−H bond, and vary from 1.689 to 1.797 Å. The ∠M^+O3PO4 dihedral angle decreases and varies from −18.6 to 6.9°.

Threshold Analysis. The model of eq 1 was used to independently analyze the thresholds for reactions 3 and 6 for all four M^+(TEP) systems. The results of these analyses are provided in Table 2. However, the M^+(DEP) product cross section is strongly affected by subsequent dissociation shortly after the threshold, such that the unaffected energy range is narrow. As a result, fits of the sum of the three products of the low-energy activated dissociation pathways (reactions 3−5) were also performed and were able to reproduce the data over a much broader energy range with good fidelity. The sum of

Table 2. Fitting Parameters of Equation 1, Threshold Dissociation Energies at 0 K, and Entropies of Activation at 1000 K of M^+(TEP) Complexes Obtained from Independent Analyses of the Simple CID and Primary Activated Dissociation Cross Sections for Elimination of Ethene[a]

species	ionic product	σ_0[b]	n[b]	E_0[c] (eV)	E_0(PSL) (eV)	E_0(TS_{6M}) (eV)	kinetic shift	$\Delta S^{\ddagger}$ (J/mol K)
Mg^+(TEP)	Mg^+(DEP)	19.1 (3.4)	1.3 (0.1)	3.41 (0.17)	–	1.56 (0.08)	1.85	−28 (1)
	Mg^+(XEP)[d]	19.7 (4.0)	1.3 (0.1)	3.47 (0.18)	–	1.55 (0.09)	1.92	−28 (1)
	Mg^+	3.0 (0.4)	1.2 (0.1)	5.76 (0.07)	2.84 (0.11)	–	2.92	19 (2)
Al^+(TEP)	Al^+(DEP)[d]	7.7 (1.6)	1.1 (0.2)	3.26 (0.15)	–	1.62 (0.11)	1.64	−9 (1)
	Al^+(XEP)	8.4 (1.9)	1.6 (0.1)	3.26 (0.15)	–	1.59 (0.12)	1.67	−9 (1)
	Al^+	1.3 (0.2)	2.1 (0.1)	5.86 (0.06)	2.87 (0.11)	–	2.99	21 (2)
Cu^+(TEP)	Cu^+(DEP)	12.9 (2.0)	0.8 (0.2)	3.74 (0.13)	–	1.75 (0.07)	1.99	−14 (1)
	Cu^+(XEP)[d]	16.0 (0.9)	1.2 (0.1)	3.77 (0.05)	–	1.72 (0.06)	2.05	−14 (1)
	Cu^+	2.1 (0.6)	1.3 (0.2)	5.16 (0.04)	2.68 (0.04)	–	2.48	34 (2)
	Cu^+[e]	2.9 (0.6)	1.1 (0.1)	5.57 (0.08)	2.77 (0.05)	–	2.80	34 (2)
Zn^+(TEP)	Zn^+(DEP)	18.6 (2.0)	0.7 (0.2)	3.81 (0.11)	–	1.78 (0.07)	2.03	−20 (1)
	Zn^+(XEP)[d]	33.7 (2.1)	0.7 (0.1)	4.06 (0.06)	–	1.77 (0.06)	2.29	−20 (1)
	Zn^+	2.1 (0.5)	1.1 (0.1)	4.90 (0.07)	2.50 (0.09)	–	2.40	28 (2)
	Zn^+[e]	3.3 (0.4)	0.8 (0.1)	5.33 (0.08)	2.63 (0.08)	–	2.70	27 (2)

[a] Uncertainties are listed in parentheses. [b] Average values for PSL or TS_{6M} TSs. [c] No RRKM analysis. [d] Fits to the sum of the three low-energy activated dissociation product cross sections (i.e., M^+(XEP) = M^+(DEP) + M^+(MEP) + M^+(P)). [e] Fits using a fixed n value derived from the competitive analyses.

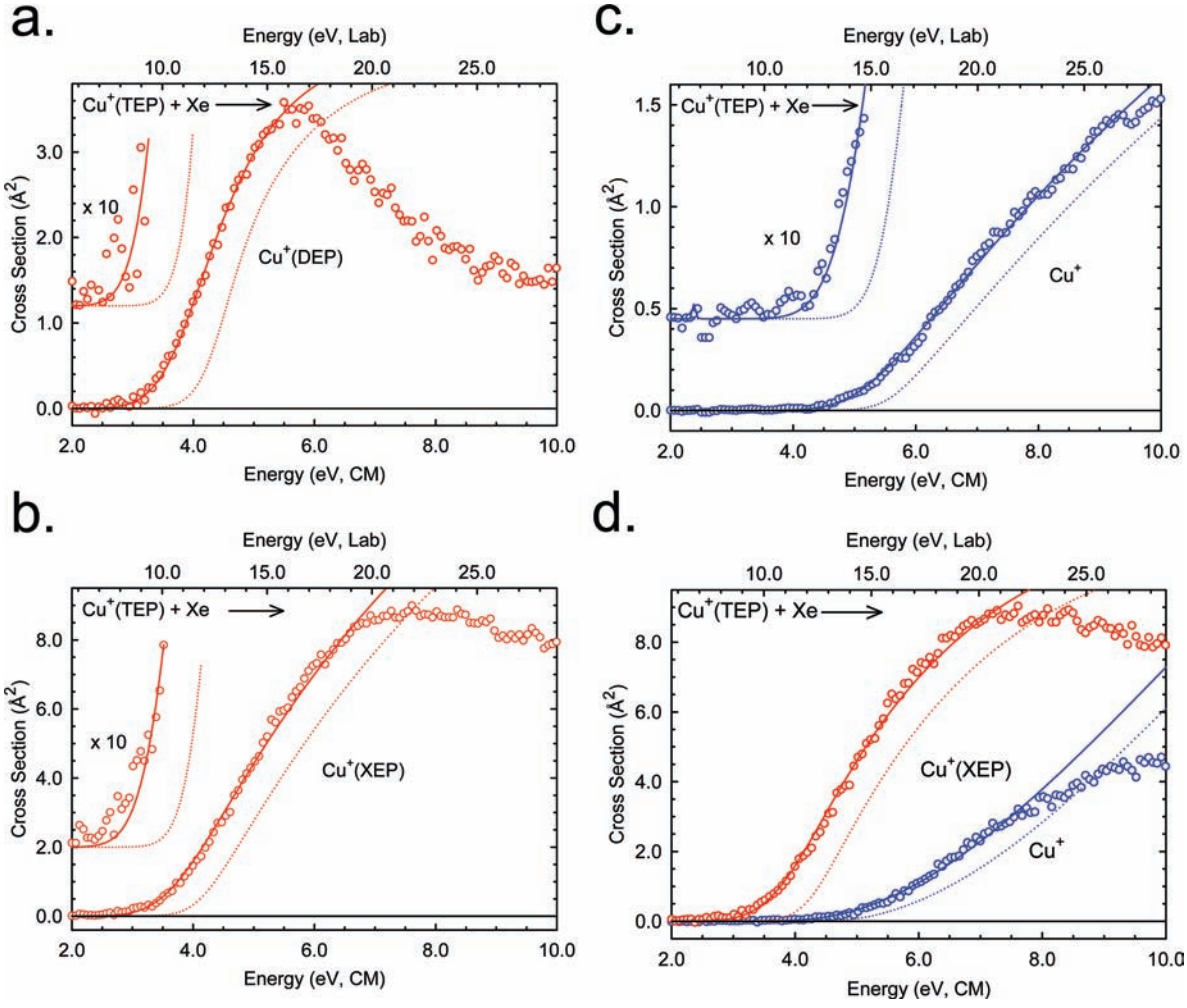

Figure 5. Zero-pressure-extrapolated Cu^+(DEP) (a), Cu^+(XEP) (b), where Cu^+(XEP) = {Cu^+(DEP) + Cu^+(MEP) + Cu^+(P)}, Cu^+ (c), and Cu^+(XEP) and Cu^+ (d) product cross sections for collision-induced dissociation of the Cu^+(TEP) complex with Xe in the threshold region as a function of kinetic energy in the center-of-mass frame (lower x-axis) and laboratory frame (upper x-axis). The solid lines show the best fits to the data using eq 1 (a−c) or eq 2 (d) convoluted over the neutral and ion kinetic and internal energy distributions. The dotted lines show the model cross sections in the absence of experimental kinetic energy broadening for reactants with an internal energy corresponding to 0 K.

the M^+(DEP), M^+(MEP), and M^+(P) product cross sections are designated as M^+(XEP). The results of these analyses are also provided in Table 2. Representative fits to the CID cross sections for the Cu^+(TEP) complex are shown in Figure 5. The other systems exhibit comparable results and are shown as Figure 4S of the Supporting Information. In all cases, the experimental cross sections for CID reactions 6 are accurately reproduced using a loose PSL TS model.[29] Previous work has shown that

Table 3. Fitting Parameters of Equation 2, Threshold Activation Energies at 0 K, and Entropies of Activation at 1000 K of M^+(TEP) Complexes Obtained from Competitive Analyses of the Simple CID and Activated Dissociation Product Cross Sections for Elimination of Ethene[a]

species	ionic product	σ_0[b]	n[b]	E_0(PSL)/(eV)	$E_0(TS_{6M})$ (eV)	competitive shift (eV)	$\Delta S^\dagger$ (J/mol·K)
Mg^+(TEP)	Mg^+(XEP)[c]	32.9 (3.0)	0.9 (0.1)	–	1.65 (0.07)	–	−28 (1)
	Mg^+	2.6 (0.4)	0.9 (0.1)	2.84 (0.12)	–	0.10	19 (2)
Al^+(TEP)	Al^+(XEP)[c]	20.9 (2.8)	0.9 (0.1)	–	1.79 (0.08)	–	−9 (1)
	Al^+	14.4 (1.7)	0.9 (0.1)	2.99 (0.11)	–	0.08	25 (2)
Cu^+(TEP)	Cu^+(XEP)[c]	18.9 (0.9)	1.1 (0.1)		1.66 (0.06)	–	−14 (1)
	Cu^+	–	1.1 (0.1)	2.72 (0.07)	–	−0.10, −0.05[d]	33 (2)
Zn^+(TEP)	Zn^+(XEP)[c]	34.7 (2.2)	0.8 (0.1)	–	1.76 (0.06)	–	−20 (1)
	Zn^+	0.7 (0.1)	0.8 (0.1)	2.71 (0.09)	–	−0.22, −0.09[d]	28 (2)

[a] Uncertainties are listed in parentheses. [b] Average values for PSL or TS_{6M} TSs. [c] Fits to the sum of the three low-energy activated dissociation product cross sections (i.e., $M^+(XEP) = M^+(DEP) + M^+(MEP) + M^+(P)$). [d] Competitive shift when the independent analysis of the M^+ channel is analyzed using a fixed n value corresponding to that found for the competitive analyses.

this model provides the most accurate assessment of the kinetic shifts for CID processes of electrostatically bound ion−molecule complexes.[29,30] The experimental cross sections for reactions 3 are modeled with tight TS models, TS_{6M} and TS_{4M}. Good reproduction of the data is obtained over energy ranges exceeding 1.5 eV and cross section magnitudes of at least a factor of 100. Although theory indicates that TS_{4M} provides the lowest energy dissociation pathway for the Al^+(TEP) complex, fits to the Al^+(DEP) cross sections provide a lower threshold energy when the TS_{6M} parameters are used to model the data. The thresholds obtained for the TS_{6M} pathway for these four M^+(TEP) complexes are lower than that derived from the TS_{4M} pathway by 12.1 ± 9.7 kJ/mol. Therefore, TS_{6M} better describes the lowest energy pathway for activation of M^+(TEP), in contrast to the theoretical results for the Al^+(TEP) complex. Table 2 also lists threshold values, E_0, obtained without including the RRKM lifetime analysis. Comparison of these values with the E_0(PSL) values shows that the kinetic shifts vary from 2.40 to 2.99 eV for fits to the M^+ product cross sections (reactions 6), while the kinetic shifts for the $E_0(TS_{6M})$ thresholds vary from 1.64 to 2.03 eV for fits to the M^+(DEP) product cross sections and 1.67 to 2.29 eV for fits to the M^+(XEP) cross sections (reactions 3), respectively.

For all four M^+(TEP) systems, competition among reactions 3 and 6 occurs and is expected to influence the threshold determinations. The cross sections for reactions 3 and 6 of Mg^+(TEP), Cu^+(TEP) and Zn^+(TEP) were analyzed competitively using the model of eq 2 (using a tight TS_{6M} TS for reactions 3 and a loose PSL TS for reactions 6). Al^+(TEP) was modeled competitively using both the TS_{4M} and TS_{6M} TSs for reaction 3 and a PSL TS for reaction 6. When the modeling included competition, the experimental cross sections for the Al^+(TEP) complex could only be accurately reproduced using TS_{6M} for reaction 3 and the PSL TS for reaction 6, consistent with the independent analyses. This again suggests that TS_{6M} is the proper pathway for the elimination of ethene from M^+(TEP) in spite of the relative energetics suggested by theory for the Al^+(TEP) complex. The results of these analyses are provided in Table 3. The M^+−TEP BDEs obtained from competitive fits are larger than the values obtained from independent fits, and are in better agreement with theoretical results for the Cu^+(TEP) and Zn^+(TEP) complexes. The BDE extracted from competitive fitting is not altered from that found for independent analyses of the Mg^+(TEP) complex. The BDE extracted from the independent analyses is in better agreement with the theoretical value for the Al^+(TEP) complex; however, the reversal of the relative energetics for TS_{6M} and TS_{4M} already indicate that theory is not capable of describing this system as well as the others. Comparison of the results obtained for the competitive and independent analyses allows the competitive shifts to be assessed. The competitive shifts vary from −0.22 to 0.10 for the M^+−TEP BDEs. The independent fits to the minor M^+ product cross sections require larger n values to reproduce the slowly rising cross sections, and therefore led to lower threshold energies. When competition is included in the analyses, the slow rising behavior is shown to be the consequence of the competition and is properly handled by a lower n value, and explains the "negative" competitive shifts observed for the Cu^+(TEP) and Zn^+(TEP) systems. If the n value for the independent analyses of reactions 6 of the Cu^+(TEP) and Zn^+(TEP) complexes is fixed at the value determined from the competitive analyses, the thresholds shift to 2.77 ± 0.05 and 2.63 ± 0.08 eV, respectively, such that the competitive shifts become −0.01 and −0.09 eV, respectively in better accord with expectations.

The entropy of activation, $\Delta S^\dagger$, is a measure of the looseness of the TS and also a reflection of the complexity of the system. It is largely determined by the molecular parameters used to model the energized molecule and the TS for dissociation, but also depends on the threshold energy. The $\Delta S^\dagger(TS_{6M})$ and $\Delta S^\dagger$(PSL) values at 1000 K for reactions 3 and 6 are listed in Tables 2 and 3, respectively. The $\Delta S^\dagger(TS_{6M})$ values at 1000 K for reaction 3 are negative and vary from and −28 to −9 J/mol·K, indicative of the tight TS for this dissociation pathway. In contrast, the $\Delta S^\dagger$(PSL) values at 1000 K for reactions 6 vary from 19 to 34 J/mol·K, indicative of fairly loose binding for this dissociation pathway.

Discussion

Trends in the Binding of Metal Cations to TEP. The 0 K BDEs of the M^+(TEP) complexes measured here are summarized in Table 4 along with the values previously determined for the M^+(TEP) complexes to Na^+ and K^+ and the corresponding theoretical BDEs.[28] The measured M^+ binding affinities follow the order: $K^+ < Na^+ < Zn^+ < Cu^+ < Mg^+ < Al^+$, indicating that the strength of the M^+−TEP interaction is dependent on the valence electronic structure of the metal cation. In contrast, theory suggests that the M^+−TEP BDEs follow the order $K^+ < Na^+ < Mg^+ < Al^+ < Zn^+ < Cu^+$.

s Orbital Occupation. In earlier work, the interaction of TEP with alkali metal cations was studied.[28] The Na^+, Mg^+, and Al^+ cations have $3s^0$, $3s^1$, and $3s^2$ electron configurations, respectively. This allows us to examine the influence of the s orbital occupation upon the binding energy. Pauli repulsion between the electron(s) on the metal cation and the oxygen lone pair increases as the occupation of the s orbital increases, suggesting that the BDEs would also decrease. In contrast, both

Table 4. Enthalpies of Metal Cation Binding to TEP at 0 K in kJ/mol

		theory		
M^+	experiment TCID	D_e[b]	D_0[b,c]	$D_{0,BSSE}$[b,d]
Na^+[e]	181.4 (5.8)	186.6	183.7	179.7
K^+[e]	135.1 (5.8)	141.1	139.2	137.8
Mg^+	274.0 (11.6)	267.3	264.5	260.5
Al^+	288.5 (10.6)	269.7	267.4	264.6
Cu^+	262.4 (6.8)	279.4	276.1	272.5
Zn^+	261.5 (8.7)	274.4	272.0	268.7

[a] Present results, competitive fitting. Uncertainties are listed in parentheses. [b] Calculated at the B3LYP/6-311+G(2d,2p)//B3LYP/6-31G* level of theory, present results. [c] Including ZPE corrections with B3LYP/6-31G* frequencies scaled by 0.9804. [d] Also includes BSSE corrections. [e] Reference 27.

Table 5. Enthalpies of Activation for Elimination of Ethene from M^+(TEP) at 0 K in kJ/mol

		theory	
species	experiment TCID[a]	AE_e[b]	AE_0[b,c]
Mg^+(TEP)	159.2 (6.8)	179.5	158.6
Al^+(TEP)	172.7 (7.7)	201.8	179.3
Cu^+(TEP)	160.2 (5.8)	184.4	161.8
Zn^+(TEP)	169.8 (5.8)	185.6	164.2

[a] Experimental and theoretical results. TS_{6M}. Uncertainties are listed in parentheses. [b] Calculated at the B3LYP/6-311+G(2d,2p)//B3LYP/6-31G* level of theory. [c] Including ZPE corrections with B3LYP/6-31G* frequencies scaled by 0.9804.

the calculated and measured BDEs are observed to increase significantly from Na^+ to Mg^+ and slightly from Mg^+ to Al^+. The enhancement in the binding in the Mg^+ and Al^+ complexes arises as a result of 3s-3p polarization.[53−56] Such hybridization polarizes the valence electron density of the metal cation away from the ligand, which requires energy but exposes a higher nuclear charge to the ligand, resulting in stronger binding. In the limit of complete removal of the valence electrons, this would correspond to binding to Mg^{2+} and Al^{3+}, consistent with the observed trend in these BDEs.

Weaker binding of Al^+ as compared to Mg^+ to ligands might be expected because two electrons must be hybridized and s-p polarization requires more energy for Al^+ than for Mg^+. However, both theory and experimental results indicate that Al^+ binds slightly stronger to TEP than Mg^+, consistent with a higher nuclear change being exposed to the TEP ligand in the Al^+(TEP) complex than the Mg^+(TEP) complex. The calculated Al^+-O3 bond length is shorter than Mg^+-O3, while the calculated Al^+-O4 bond length is longer than Mg^+-O4, indicating Al^+ favors binding to the oxo oxygen to a greater extent than Mg^+, which has more electron density and enhances the Al^+ binding to TEP.

s,d Orbital Occupation. Both theory and experiment agree that Cu^+ and Zn^+ bind TEP much more strongly than K^+, the $4s^0$ cation of the same periodic row. The strong binding to Cu^+ and Zn^+ arises as a result of the involvement of the valence electrons in the binding and the mechanisms by which these transition metal cations are capable of decreasing Pauli repulsion between the metal cation and phosphate ester. These mechanisms include: 4s-4p polarization and 4s-3dσ hybridization. Because the 4p orbitals lie higher in energy than the 3d orbitals, 4s-4p polarization requires more energy than 4s-3dσ hybridization. The valence electron configuration of Cu^+ is $3d^{10}$. The 4s orbital is empty and 4s-3dσ hybridization hybridizes electron density away from the TEP ligand and places that electron density in a direction perpendicular to the bonding axis. The electron configuration of Zn^+ is $4s^13d^{10}$ such that the 4s orbital is occupied. Thus, Zn^+ cannot use sd hybridization, but Zn^+ can benefit from s-p polarization. The 4s-4p polarization is analogous to the mechanism observed in the Mg^+ and Al^+ systems in that it polarizes electron density to the opposite side of the metal cation away from the ligand, allowing the ligand to experience a larger effective nuclear charge. Therefore, Cu^+ is expected to bind TEP more strongly than Zn^+ as a result of decreased Pauli repulsion associated with the occupied 4s orbital of Zn^+, and the less energetic mechanism for reducing the Pauli repulsion for Cu^+, consistent with both the theoretical calculations and experimental measurements.

Trends in the Activation of TEP to Eliminate C_2H_4 by Metal Cation Binding. The 0 K AEs of the M^+(TEP) complexes measured here are summarized in Table 5. Low-energy activated dissociation leading to the elimination of C_2H_4 is observed and corresponds to the lowest energy pathway for all four systems. The thresholds for this activation process are similar and vary between 159.2 and 172.7 kJ/mol, and follow the order: $Mg^+ < Cu^+ < Zn^+ < Al^+$. It is slightly easier for Mg^+ and Cu^+ than for Zn^+ and Al^+ to activate TEP, while there is no apparent correlation between the BDEs and AEs for these four M^+(TEP) complexes. When no metal cation is bound to TEP, the TS_{6M} is calculated to lie 154.1 kJ/mol above the ground state conformation of TEP. Therefore, it seems that all four metal cations examined here actually slightly to moderately inhibit the activated dissociation of TEP to eliminate ethene. The valence electron configurations of Mg^+, Al^+, Cu^+, and Zn^+ are s^1, s^2, d^{10}, and s^1d^{10}, respectively. Thus the valence s electrons and a full d shell are not effective activators of the phosphate ester bond of TEP. However, the binding of these metal cations provides a mechanism by which mass spectrometry can be used to characterize the activated dissociation and activation propensities of the metal cations. More complicated dissociation behavior was observed for the M^+(TEP) complexes to Li^+ and other transition metal cations, including additional and even lower energy activated dissociation pathways. These results indicate that these metal cations exhibit greater activation propensities and will be the subject of future manuscripts.

Comparison of Theory and Experiment. The M^+-TEP BDEs and AEs for elimination of ethene from M^+(TEP) at 0 K were calculated at the B3LYP/6-311+G(2d,2p)//B3LYP/6-31G* level of theory including ZPE and BSSE corrections. The theoretical BDEs and AEs of the M^+(TEP) complexes are summarized in Tables 4 and 5, respectively, along with the measured values. Excellent agreement between the theoretical and the TCID experimental results is obtained for the AEs of these complexes, while somewhat less satisfactory agreement is found for the BDEs. For simple CID, the BDEs from competitive modeling are in better agreement with theoretical results than values derived from independent analyses as expected. The mean absolute deviation (MAD) between theory and experiment for the BDEs obtained from competitive analyses is 13.7 ± 7.3 kJ/mol, smaller than that from independent analyses, 16.8 ± 7.2 kJ/mol (and 11.5 ± 4.3 kJ/mol for fits with fixed n values).

(53) Bauschlicher, C. W.; Langhoff, S. R.; Partridge, H. *J. Chem. Phys.* **1991**, *94*, 2068.
(54) Bauschlicher, C. W.; Langhoff, S. R.; Partridge, H.; Rice, J. E.; Komornicki, A. *J. Chem. Phys.* **1991**, *95*, 5142.
(55) Bauschlicher, C. W.; Partridge, H. *J. Chem. Phys.* **1991**, *95*, 9694.
(56) Bauschlicher, C. W.; Sodupe, M.; Partridge, H. *J. Chem. Phys.* **1992**, *96*, 4453.

The average experimental uncertainty (AEU) for the results of the competitive analyses is 9.4 ± 2.1 kJ/mol, slightly larger than that for independent analyses, 8.5 ± 3.2 kJ/mol (and 8.4 ± 2.8 kJ/mol for fits with fixed *n* values). The large difference in the experimental and theoretical BDE for the Al^+(TEP) complex is the major contributor to the MADs. If this value is not included, the MAD drops to 10.3 ± 3.2 kJ/mol, only slightly larger than the AEU, 9.0 ± 2.4 kJ/mol. The MAD between theory and experiment for the AEs is 3.6 ± 2.9 kJ/mol, smaller than that from the independent analyses 11.4 ± 9.8 kJ/mol for fits to M^+(XEP) and 11.5 ± 7.7 kJ/mol for the fits to M^+(DEP). The AEU for the results of the competitive analyses is 6.5 ± 0.9 kJ/mol, smaller than that from the independent analyses, 8.0 ± 2.8 kJ/mol for fits to M^+(XEP) and 8.0 ± 1.8 kJ/mol for fits to M^+(DEP). As discussed above, theory indicates that TS_{4M} provides a lower energy dissociation pathway for Al^+(TEP), whereas our experimental results suggest that the TS_{6M} is the most favorable pathway. Therefore, our experimental results provide a more reliable determination of the energetics of the activated dissociation processes.

Conversion from 0 to 298 K. The 0 K AEs for elimination of ethene from M^+(TEP) and the M^+−TEP BDEs determined here are converted to 298 K activation and bond enthalpies and free energies to allow comparison to literature values and commonly employed experimental conditions. The conversions are calculated using standard formulas (assuming harmonic oscillator and rigid rotor models) using the vibrational frequencies and rotational constants determined for the B3LYP/6-31G* optimized geometries as listed in Tables 1S and 2S (Supporting Information). Tables 8S and 9S (Supporting Information) list the 0 and 298 K enthalpy, free energy, and enthalpic and entropic corrections for all M^+(TEP) complexes experimentally and theoretically determined (from Tables 4 and 5). Uncertainties are determined by 10% variation in the molecular constants.

Comparison of Metal Cation Binding to TEP and the Nucleobases. Both the phosphate groups along the backbone and the nucleobases are important metal cation binding sites in nucleic acids. Comparison of metal cation binding to TEP and the nucleobases should provide insight into the binding preferences of metal cations to nucleic acids and provide a better understanding of how cation binding influences the structure and stability of phosphate esters in the gas phase. However, the phosphate groups along the backbone of nucleic acids can be neutral or deprotonated in the gas phase. Deprotonation of the phosphate group should enhance its metal cation binding affinity. Thus, cations that bind more strongly to TEP than the nucleobases should bind to the phosphate backbone of nucleic acids regardless of its state of protonation. The preferred site of binding to nucleic acids of cations that bind less strongly to TEP than the nucleobases could however be influenced by its state of protonation.

The gas phase alkali metal cation (Li^+, Na^+, and K^+) binding affinities of the nucleobases were determined using TCID[22] and the kinetic method[21] and were found to follow the order: G > C > A > T ∼ U. TCID was also used to measure the BDEs of Na^+ and K^+ to TEP.[28] TEP was found to bind Na^+ and K^+ more strongly than the four nucleobases. This can be explained by the electrostatic nature of the binding. The alkali metal cation binding strength is mainly determined by the bond length. Although Na^+ and K^+ bind to the nucleobases in a multidentate fashion, alkali metal cations cannot achieve optimal binding geometries because the structures of the nucleobases are more rigid than TEP. The relative alkali metal cation affinities of TEP and the nucleobases may also be understood by comparison of the polarizabilities (16.42 Å^3 for TEP vs 14.77, 11.03, 13.10, 11.23, and 9.69 Å^3 for G, C, A, T, and U, respectively) and the dipole moments of TEP and the nucleobases (1.28 D for TEP vs 2.04, 3.72, 4.98, 5.11, 2.54 D, for G, C, A, T, and U, respectively). The polarizability of TEP is 25.3% larger than that for adenine, while the dipole moment of TEP is 49.6% smaller than that of adenine. Thus, the BDEs are dominated by the metal cation-induced dipole interaction. The BDEs of Mg^+ to U and T were measured to be 211.3 and 213.2 kJ/mol,[23] much smaller than the BDE of the Mg^+(TEP) complex measured here, 274.0 ± 11.6 kJ/mol. The relative metal cation binding affinities to the four nucleobases varies between 17 and 34 kJ/mol for the complexes to Li^+, Na^+, and K^+.[21] Therefore the binding of Mg^+ to TEP is expected to be stronger than to the other nucleobases (G, C, and A). Similar behavior is expected for Al^+ because it only possesses one more electron than Mg^+ and employs the same mechanism for reducing Pauli repulsion. Therefore, in the gas phase the alkali metal cations, Mg^+, and Al^+ are expected to bind preferentially to the phosphate group of nucleic acids regardless of its state of protonation.[7]

A comparison of Cu^+ binding to TEP and A[24,26] indicates that the binding to TEP is weaker than to adenine. This trend differs from that for Na^+, K^+, Mg^+, and Al^+. The binding of these two ligands to Cu^+ is more covalent in nature than to Na^+, K^+, Mg^+, and Al^+ as a result of the participation of the valence d electrons in the binding. In the gas phase, the metal cation binding affinities of the nucleobases follow the order: G > C > A > T ∼ U.[21,22,24,26] As noted above, the binding of Cu^+ to TEP is weaker than to adenine. Thus, G and C should bind Cu^+ more strongly, while T and U should bind Cu^+ less strongly, than TEP. Therefore, in the gas phase Cu^+ is expected to preferentially bind to A, C, and G nucleobases when the phosphate groups are neutral. However, it is unclear whether Cu^+ would preferentially bind to these nucleobases or the phosphate backbone of nucleic acids when deprotonated. Therefore, the state of protonation and base composition of nucleic acids may also strongly influence the preference for phosphate versus nucleobase binding: A, C, and G regions likely favor base binding, while T and U regions should favor binding to the phosphate backbone.

Implications for Metal Cation Binding to Nucleic Acids in Condensed Phases. In condensed phases, metal cation-nucleic acid interactions are complicated by intermolecular and solvation interactions. In crystal structures, alkali metal cations bind in an asymmetric fashion to the deprotonated phosphate group indicating that the interaction with water molecules is more favorable than a bidentate interaction with the phosphate group as found for the isolated M^+(TEP) complexes examined here. The interaction of the metal cation with additional water molecules in the condensed phase should further weaken the metal cation-phosphate ester interactions as compared to the isolated species in the gas phase.[57,58] This suggests that alkali metal cation-phosphate ester interactions in solution are likely intermediate between the gas phase interactions of alkali metal cations with the corresponding neutral and deprotonated phosphate esters. According to a quantum chemical and molecular dynamics study,[59] 80% of Na^+ cations are almost entirely

(57) Schneider, B.; Kabelac, M. *J. Am. Chem. Soc.* **1998**, *120*, 161.
(58) Schneider, B.; Kabelac, M; Hobza, P. *J. Am. Chem. Soc.* **1996**, *118*, 12207.
(59) Laughton, C. A.; Luque, F. J.; Orozco, M. *J. Phys. Chem.* **1995**, *99*, 11591–11599.

associated with the phosphate group of DNA and are approximately equally distributed between its first and second solvation shells. This indicates that alkali metal cation binding to the phosphate ester is stronger than to water, ensuring that alkali metal cations effectively bind and contribute to the structural stabilization of nucleic acids.

Similar analogies can likely be drawn for Cu^+. Interaction with water molecules should alter the strength and geometry of binding to both the nucleobases and phosphate groups. However, stabilization of the negative charge of the phosphate group by solvent molecules likely helps to preserve the preference for binding to A, C, and G nucleobases over the phosphate backbone. Thus, Cu^+ binding to nucleic acids likely contributes to their destabilization and degradation.

Direct analogies for the other metal cations examined here, Mg^+, Al^+, and Zn^+, are not possible because in solution these metals are found as Mg^{2+}, Al^{3+}, and Zn^{2+}. In their natural oxidation states these metals should bind to the phosphate groups and nucleobases much more strongly as a result of their higher nuclear charge, but would also bind solvent molecules more strongly. It is known that Mg^{2+} binding to DNA in solution is found to stabilize the structure and increase the melting temperature by neutralizing negative charges on the phosphate backbone.[60] In solution, the preference for phosphate over base association was estimated by measuring the melting temperature after metal cation binding and found that the preference decreases in the order: $Mg^{2+} > Zn^{2+} > Cu^{2+}$.[9] This is consistent with the gas phase trend discussed above for the monocations. It seems likely that Al^{3+} would exhibit an even greater preference for the phosphate backbone as a result of higher nuclear charge. Therefore, although the M^+(TEP) complexes investigated here in the gas phase are not of direct physiological relevance, the trends in the binding parallel that for the dications and thus they still provide useful insight into the influence of metal cationization on the structure and stability of nucleic acids.

Conclusions

Results from kinetic energy dependent CID studies of four M^+(TEP) complexes with Xe, where $M^+ = Mg^+$, Al^+, Cu^+, and Zn^+, clearly show that activated dissociation of the phosphate ester bonds resulting in the sequential elimination of ethene molecules is strongly favored over loss of the intact TEP ligand. The thresholds for these activated dissociation and simple CID pathways are interpreted to yield AEs for elimination of C_2H_4 from M^+(TEP) and M^+-TEP BDEs, respectively. Theoretical calculations performed at the B3LYP/6-311+G(2d,2p)//B3LYP/6-31G* level of theory are employed to characterize the structures, energetics, and detailed reaction mechanisms for the observed dissociation pathways. Elimination of ethene from all four M^+(TEP) complexes is found to proceed via a 6-membered ring transition state. The agreement between theory and experiment for the AEs is excellent for all complexes and reasonably good for the BDEs for most complexes. Comparison of metal cation−TEP binding with metal cation-nucleobase binding indicates that Na^+, K^+, Mg^+, and Al^+ bind more strongly to TEP than to the nucleobases. These results are consistent with the fact that in solution "hard" metal cations favor binding to the phosphate backbone of nucleic acids and indicate that interactions with solvent do not significantly alter their binding trends and preferences. The binding of Cu^+ to TEP is weaker than to A, which binds metal cations less strongly than C and G. The preference for Cu^+ to bind to the nucleobases over the phosphate backbone of nucleic acids again suggests that interactions with solvent do not significantly alter its binding preferences.

Acknowledgment. This work is supported by the National Science Foundation, Grant CHE-0528262. We also thank the Wayne State University C&IT for computer time.

Supporting Information Available: Tables of vibrational frequencies and average vibrational energies at 298 K, rotational constants, Cartesian coordinates of the B3LYP/6-31G* optimized geometries for all species associated with the activated dissociation and simple CID of the M^+(TEP) complexes, geometrical parameters for TEP, M^+(TEP), TS_{6M}, and TS_{4M}, and enthalpies and free energies of activated dissociation to eliminate ethene and for binding of these metal cations to TEP at 298K; figures giving cross sections for collision-induced dissociation, optimized ground state structures of M^+(TEP) complexes, potential energy maps for the TS_{6M} and TS_{4M} dissociation pathways, and thermochemical analyses of the zero-pressure extrapolated collision-induced dissociation cross sections. This material is available free of charge via the Internet at http://pubs.acs.org.

JA8092357

(60) Eichhorn, G. L. *Metal Ions in Genetic Information Transfer*; Elsevier: New York, 1981; Vol. 1.